THE ASTROPHYSICAL JOURNAL, 561:299–307, 2001 November 1
© 2001. The American Astronomical Society. All rights reserved. Printed in U.S.A.

SCATTERED LIGHT MODELS OF PROTOSTELLAR ENVELOPES: MULTIPLE OUTFLOW CAVITIES AND MISALIGNED CIRCUMSTELLAR DISKS

KENNETH WOOD,[1,2] DAVID SMITH,[3] BARBARA WHITNEY,[4] KEIVAN STASSUN,[5] SCOTT J. KENYON,[1]
MICHAEL J. WOLFF,[4] AND KAREN S. BJORKMAN[6]
Received 2001 March 29; accepted 2001 June 29

ABSTRACT

Ground-based imaging, imaging polarimetry, and recent *Hubble Space Telescope* WFPC2 and NICMOS images of protostars have revealed very complex scattered light patterns that cannot be entirely explained by two-dimensional radiation transfer models. We present here for the first time radiation transfer models of T Tau and IRAS 04016+2610 that are fully three-dimensional, with the aim of investigating the effects on image morphology of multiple illuminating sources and infalling envelopes that have been shaped by multiple outflows. For T Tau we have constructed scattered light models where the illumination of the surrounding envelope is by a binary, with each source surrounded by its own small circumstellar disk or envelope. We find that the asymmetries in the WFPC2 image of T Tau can be reproduced if the disks in the binary system are misaligned, consistent with a recently discovered bipolar outflow believed to originate from the secondary. For IRAS 04016+2610 we find that the observed scattered light pattern can be reproduced by scattering in an envelope with cavities carved by two sets of bipolar outflows, suggestive of an embedded binary system.

Subject headings: circumstellar matter — dust, extinction — ISM: jets and outflows — radiative transfer — stars: formation — stars: individual (T Tauri, IRAS 04016+2610)

1. INTRODUCTION

In the standard picture of low-mass star formation (see, e.g., Shu, Adams, & Lizano 1987), Class I protostars are young sources (age $\sim 10^5$ yr) that are still surrounded by massive ($\sim 0.01\ M_\odot$) circumstellar disks and partly obscured by their natal envelopes. These stars appear highly extincted in the optical, with spectral energy distributions that peak in the mid- to far-infrared (see, e.g., Lada & Wilking 1984; Beichman et al. 1986; Lada 1987; Myers et al. 1987; Wilking, Lada, & Young 1989; Kenyon et al. 1990; Kenyon, Calvet, & Hartmann 1993a), and exhibit highly polarized reflection nebulae (see, e.g., Whitney & Hartmann 1993; Whitney, Kenyon, & Gómez 1997; Lucas & Roche 1997, 1998). From observations of Class I protostars has emerged a coherent picture of the protostellar environment. The basic model consists of a dusty infalling envelope with cavities carved by the energetic outflows associated with this phase of star formation. The envelope absorbs the optical light and emits this radiation at longer wavelengths (see, e.g., Adams & Shu 1986; Adams, Lada, & Shu 1987; Kenyon et al. 1993a); the reflection nebulae are formed by starlight scattering off the cavity walls (Bastien & Ménard 1990; Tamura et al. 1991; Whitney & Hartmann 1993; Kenyon et al. 1993b; Whitney et al. 1997; Lucas & Roche 1997, 1998; Lucas, Blundell, & Roche 2000; Reipurth et al. 2000).

Using this basic picture as a foundation, models have been constructed, including disks, envelopes, and bipolar cavities, that can reproduce in gross detail the observed spectral energy distributions and low-resolution ground-based imaging of many Class I sources (Whitney & Hartmann 1992, 1993; Whitney et al. 1997; Fischer, Henning, & Yorke 1994; Lucas & Roche 1997, 1998; Stapelfeldt et al. 1998b). However, detailed agreement between these models and the observed scattered light patterns of many Class I sources has been less forthcoming, in large part because the existing two-dimensional models have necessarily assumed axisymmetric circumstellar geometries. High-resolution *Hubble Space Telescope* (*HST*) images show that many sources exhibit very complicated scattered light patterns indicative of nonaxisymmetric geometries and/or illumination (Burrows et al. 1996; Padgett et al. 1999; Stapelfeldt et al. 1995, 1998a, 1998b, 1999; Terebey et al. 1998; Hartmann et al. 1999; Krist et al. 1998, 1999; Reipurth et al. 2000). Recent imaging polarimetry has provided additional compelling evidence that some sources exhibit departures from an axisymmetric disk-envelope-cavity system (Whitney et al. 1997; Lucas & Roche 1997, 1998; Lucas et al. 2000).

Two particularly good examples of sources with nonaxisymmetric circumstellar geometries are T Tauri and IRAS 04016+2610. Ground-based near-IR imaging polarimetry of IRAS 04016+2610 indicates *two* sets of bipolar outflow cavities (Lucas & Roche 1997), and *HST*/NICMOS images show the complex scattered light pattern at higher resolution (Padgett et al. 1999). Ground-based *J*, *H*, and *K* images of T Tau (Weintraub et al. 1992) were modeled by Whitney & Hartmann (1993) with a standard envelope plus bipolar cavity system, but the WFPC2 images (Stapelfeldt et al. 1998b) and near-IR adaptive optics images (Roddier et al. 1999, 2000) clearly show nonaxisymmetric nebulosity.

Motivated by these observed departures from axisymmetry, in this paper we develop scattered light models for IRAS 04016+2610 and T Tauri that for the first time

[1] Harvard-Smithsonian Center for Astrophysics, 60 Garden Street, Cambridge, MA 02138; kwood@cfa.harvard.edu, kenyon@payne.harvard.edu.
[2] School of Physics and Astronomy, University of St. Andrews, North Haugh, St. Andrews, Fife KY16 9AD, Scotland, UK; kw25@st-andrews.ac.uk.
[3] Astronomy Department, University of Texas at Austin, Austin, TX 78712; dss@astro.as.utexas.edu.
[4] Space Science Institute, Suite 23, 1540 30th Street, Boulder, CO; bwhitney@colorado.edu, wolff@colorado.edu.
[5] Astronomy Department, University of Wisconsin-Madison, 475 North Charter Street, Madison, WI 53706; keivan@astro.wisc.edu.
[6] Ritter Observatory, Department of Physics and Astronomy, University of Toledo, Toledo, OH 43606; karen@astro.utoledo.edu.

include three-dimensional geometries and illumination by multiple sources. We demonstrate that including the effects of multiple illumination sources, multiple outflow cavities, and misaligned circumstellar disks can explain the observed scattered light patterns much more fully than has been possible with two-dimensional modeling efforts hitherto. We have not undertaken an exhaustive search of parameter space when modeling the two objects, because such investigations have been presented previously for axisymmetric models (Whitney & Hartmann 1993; Kenyon et al. 1993b; Whitney et al. 1997). For our models we adopt protostellar envelope parameters derived from previous two-dimensional modeling of scattered light images and spectral energy distributions of T Tau and IRAS 04016+2610. The effects of changing the envelope parameters (e.g., accretion rate, centrifugal radius, and inclination) have been described in the aforementioned papers, and our focus is on the departures from axisymmetry required to obtain a better match between the scattered light models and data. Furthermore, since we view our models as a first step toward unraveling the complexities of the scattered light patterns, we have not attempted to quantify any figure of merit for model fits to the data. Rather, the models we present are the first numerical simulations of published suggestions as to the origin of the asymmetric scattered light patterns of the two sources. In § 2 we describe the scattered light images that form the basis for our modeling, in § 3 we describe the ingredients of our models, in § 4 we present the models for the individual sources, and we conclude in § 5 with a discussion of our findings and further observational tests of our suggested geometries.

2. SCATTERED LIGHT IMAGES

The NICMOS data (F110W, F160W, F187W, F205W) for IRAS 04016+2610 were presented by Padgett et al. (1999) and the WFPC2 data (F555W) on T Tau by Stapelfeldt et al. (1998b).

The reduced and PSF–subtracted F555W image of T Tau was provided to us by Karl Stapelfeldt. For IRAS 04016+2610 the NICMOS data were obtained from the *HST* archive and were rereduced using the IRAF[7] STSDAS package with the most recent set of reference files available. We created bad-pixel masks using the data-quality frames associated with each image, manually masking transient bad pixels, and we also manually masked the bad column 128 (Bergeron & Skinner 1997). The subsets of each image association were registered and combined using the IRAF STSDAS pipeline CALNICB task.

In order to subtract the point-spread function (PSF) from each of the recalibrated *HST* images, we rebinned the images by a factor of 2 and deconvolved them using PSFs computed with Tiny Tim version 4.4 (Krist 1995), which were also oversampled by a factor of 2. The deconvolution was performed within IRAF using the STSDAS LUCY task, which uses a Richardson-Lucy–based algorithm. The deconvolution process is an iterative one, and we stopped the process after five iterations in the F110W filter, 10 iterations in F160W, 15 iterations in F187W, and 20 iterations in F205W.

For IRAS 04016+2610 we also obtained an *I*-band image using the WIYN[8] telescope's CCD imager. The WIYN observations were obtained on 1995 December 13/14 using the WIYN imager camera, as part of a feasibility study conducted under the WIYN queue observing program. Conditions during the night were good, with some light cirrus and seeing of 0.″8–1.″4. Observations were made in each of the *VRI* bands, consisting of three 300 s exposures in each band. Offsets of 10″ were made between each exposure. The data were reduced using the standard IRAF data reduction packages for CCD images. After reduction, the individual images for each exposure were combined into one image (900 s total exposure) for each band. Here we report only *I*-band results (the morphology seen at *V* and *R* is similar). The combined *I*-band image is shown in Figure 4*a*.

3. MODEL INGREDIENTS

In this section we present the basic ingredients of the three-dimensional radiation transfer code used to model T Tau and IRAS 04016+2610. The code is comprehensive and necessarily involves a large number of parameters that in principle can be tuned to match observations. Wherever possible, we constrain our model parameters based on known properties of the sources.

The basic geometry we consider consists of an infalling envelope with bipolar cavities, illuminated from within by a single source or a binary system. For binary illumination, the two components possess circumstellar disks that are not necessarily aligned with one another or with the envelope's rotation axis.

3.1. *Envelope Geometry*

Of the two sources we model in this paper, T Tau is a known binary (Dyck, Simon, & Zuckerman 1982), and IRAS 04016+2610 shows evidence for binarity with possibly two bipolar outflow cavities (Lucas & Roche 1997). Despite the binary nature of the sources, we adopt the rotational collapse geometry of Terebey, Shu, & Cassen (1984, hereafter TSC) developed for single-star systems. We thus, in effect, assume that the circumbinary density is given by the TSC solution and neglect the effects of binary motion on the envelope structure. The focus of our present study is the three-dimensional nature of the cavities and envelope illumination; future studies may include circumbinary density distributions predicted from binary star formation models.

The TSC envelope density used in our simulations is given by

$$\rho = \frac{\dot{M}}{4\pi}\left(\frac{GM}{r_c^3}\right)^{-1/2}\left(\frac{r}{r_c}\right)^{-3/2}\left(1+\frac{\mu}{\mu_0}\right)^{-1/2} \times\left(\frac{\mu}{\mu_0}+\frac{2\mu_0^2 r_c}{r}\right)^{-1}, \quad (1)$$

where $\dot{M}$ is the mass infall rate, r_c is the centrifugal radius, $\mu = \cos\theta$, and $\mu_0 = \mu(r\rightarrow\infty)$ is determined by

$$\mu_0^3 + \mu_0(r/r_c - 1) - \mu(r/r_c) = 0 . \quad (2)$$

For our models, we vary $\dot{M}$ and r_c, in the range $\dot{M} = (2\text{–}10) \times 10^{-6}\ M_\odot\ \mathrm{yr}^{-1}$ and $r_c = 50\text{–}100$ AU (Strom 1994;

[7] IRAF is distributed by the National Optical Astronomy Observatory, which is operated by the Association of Universities for Research in Astronomy, Inc. under cooperative agreement with the NSF.

[8] The WIYN Observatory is a joint facility of the University of Wisconsin-Madison, Indiana University, Yale University, and the National Optical Astronomy Observatory.

Kenyon et al. 1993b; Whitney et al. 1997). Our radiation transfer code uses a linear Cartesian grid (§ 3.5), and in order to resolve the TSC density structure we adopt an outer radius for the envelope of 1500 AU. We note that in the models of Whitney & Hartmann (1993) and Whitney et al. (1997), outer radii of around 10,000 AU were adopted. We have found that while our smaller envelopes can reproduce the overall morphology of the scattered light images, larger envelopes produce redder colors (see the IRAS 04016+2610 models in § 4.2).

3.2. *Cavity Geometries*

We explore three-dimensional geometries by carving cavities in the axisymmetric TSC envelope. By virtue of being two-dimensional, previous modeling (see, e.g., Whitney & Hartmann 1993; Whitney et al. 1997; Lucas & Roche 1997; Stapelfeldt et al. 1998b) used bipolar cavities that were aligned with the envelope's rotational axis. In our models we adopt the same cavity shapes as used previously but now allow the cavities to be offset from the envelope's symmetry axis and also allow for the existence of multiple sets of cavities, as might result in a binary system.

We consider three cavity shapes in our modeling: streamlined, cylindrical, and curved. In the streamlined cavity shape, the cavity walls trace out the trajectory of an infalling particle as given in the TSC envelope solution. This cavity shape is approximately conical at large radii but at small radii becomes more curved. The curvature increases the cross section of the cavity walls exposed to direct starlight and results in more scattering than a purely conical shape and, consequently, in a brighter cavity (see Whitney & Hartmann 1993). Cylindrical cavities have straight walls parallel to the outflow axis. Curved cavities take the form $z = a\omega^b$ (see, e.g., Stapelfeldt et al. 1998b), where $\omega = (x^2 + y^2)^{1/2}$ and a and b are parameters that can be adjusted to provide a good match to the data or to approximate an opening angle of a molecular outflow. We also allow for the presence of dust within the cavities.

3.3. *Illumination*

As stated above (§ 3.1), T Tau is a binary, and there are indications that IRAS 04016+2610 may also be a binary. Therefore, we assume that the illumination is by binary star-plus-disk systems as used by Wood, Crosas, & Ghez (1999) in their scattered light model of GG Tau's circumbinary disk. In this model we assume two point sources of illumination, but with the radiation angular distribution of a star-plus-disk system. In this approximation we do not explicitly treat the radiation transfer through the circumstellar disks but assign an angular distribution for the flux emerging from the star-plus-disk systems. The angular dependence of the illumination of these star-plus-disk systems is displayed in Figure 1, showing the small emergent flux level at high inclinations due to the dense equatorial disk (Whitney & Hartmann 1992). The angular distribution of the illuminating sources was set up so that the sources would be at the center of the cavities, with the polar direction of the illumination pattern aligned with the cavity axis.

3.4. *Dust Opacity and Scattering Parameters*

As with previous modeling of Taurus protostars (Kenyon et al. 1993b; Whitney et al. 1997), we adopt the albedo, opacity, and scattering parameters for a Kim, Martin, & Hendry (1994, hereafter KMH) grain mixture, typical of grains in the interstellar medium (ISM). The scattering phase function is assumed to be a Henyey-Greenstein phase function (Henyey & Greenstein 1941) with asymmetry parameter g. In more evolved disk systems the spectral index and level of the long wavelength continuum emission provides strong evidence of dust grains that are larger than ISM grains (Beckwith et al. 1990; Beckwith & Sargent 1991). However, Whitney et al. (1997) found that the KMH parameters gave a good match to the colors and sizes of images Class I sources, but that they underestimated the polarization level. The KMH wavelength-dependent opacity and scattering parameters we adopt in this paper are presented in Table 1.

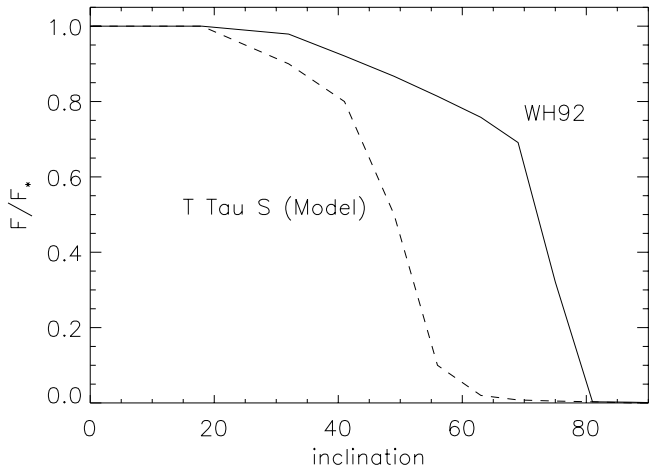

FIG. 1.—*Solid line*: Angular dependence of emerging flux from a T Tauri star-plus-disk system as determined by Whitney & Hartmann (1992). *Dashed line*: The more polar-concentrated angular distribution adopted for our modeling of T Tau S in Fig. 2*d*.

3.5. *Radiation Transfer*

We perform the radiation transfer with a Monte Carlo code that allows for arbitrary sources of emission and multiple scattering within an arbitrary geometry. The scattering code is based on that described by Code & Whitney (1995), but it has now been modified to run on a three-dimensional, linear, Cartesian grid (Wood & Reynolds 1999) and includes forced first scattering (Witt 1977) and a "peeling off" procedure (Yusef-Zadeh, Morris, & White 1984). These modifications enable us to construct model images of three-dimensional systems from specified viewing angles very efficiently. We have tested our three-dimensional code against results from the axisymmetric code of Whitney & Hartmann (1993), finding excellent agreement between the two codes.

The output of each Monte Carlo simulation is a two-dimensional image including the spatially resolved polar-

TABLE 1

PARAMETERS FOR DUST GRAINS

Wave Band	κ (cm^2 g^{-1})	a	g	P
V	219	0.54	0.44	0.43
I	105	0.50	0.35	0.51
J	65	0.46	0.32	0.58
H	38	0.42	0.29	0.59
K	22	0.36	0.25	0.60

ization (Stokes I, Q, and U images). In order to compare our models with the observations, we convolve our high-resolution models with appropriate PSFs using the Tiny Tim software (Krist 1995). From these images we calculate the integrated polarization, and by combining simulations at different wavelengths we calculate colors for comparison with observations. The colors we compute are subject to a normalization set by the intrinsic color of the illuminating source(s). The observed color is $J-H=(J'-H')+(J_0-H_0)$, where J_0-H_0 is the source color and $J'-H'$ is the color of the Monte Carlo simulation. In their simulations, Whitney et al. (1997) adopted source colors for a typical M0 T Tauri star plus reprocessing disk from Kenyon et al. (1994), $J_0-H_0=0.77$ and $H_0-K_0=0.43$. In our models of IRAS 04016+2610 we adopt the same source colors. However, for T Tau the spectral type is K0 or earlier, and because we are modeling only the WFPC2 F555W image the intrinsic source colors are not required.

4. RESULTS

In this section we present our models for T Tau and IRAS 04016+2610. Because our aim in this paper is to demonstrate the usefulness of our three-dimensional modeling method, we report here on those models that best reproduce the observed scattered light images and discuss the salient properties of those models. As we discuss in detail for each source, we constrain the parameters of our models based on the available data from the literature. Nonetheless, the uniqueness of the models presented is not demonstrated. These models should be regarded as existence proofs and as suggestions for more detailed three-dimensional investigations of these and other Class I sources in the future.

4.1. *T Tauri*

4.1.1. *Previous Two-dimensional Models and Evidence for Source Asymmetry*

T Tau is a binary star with one component seen directly and the secondary (0.″7 distant) only detected at IR and longer wavelengths (Dyck et al. 1982; Ghez et al. 1991). The bolometric luminosities of the sources are estimated to be 9 $L_\odot$ for the primary (Ghez et al. 1991) and up to 14 $L_\odot$ for the secondary (Cohen, Emerson, & Beichman 1989). Therefore, although undetected at optical wavelengths, the secondary may be emitting a lot of radiation that we only observe when it is scattered into our sight line. The optical light of the secondary may either be obscured by its location within a dense circumbinary envelope or occulted by its own circumstellar disk edge-on to our line of sight. The WFPC2 scattered light pattern shows departures from axisymmetry, with one side of the cavity appearing brighter than the other (Fig. 2*a*; Stapelfeldt et al. 1998b). A similar asymmetric scattered light pattern is seen in the near-IR adaptive optics images of Roddier et al. (1999).

The radial distribution of the near-IR scattered light surrounding T Tau (Weintraub et al. 1992) was modeled by Whitney & Hartmann (1993) adopting a near pole-on orientation of a TSC envelope ($\dot{M}=2\times10^{-6}\ M_\odot\ \mathrm{yr}^{-1}$, $r_c=100$ AU) and evacuated bipolar cavities. They found that cavities with streamlined shapes give too steep a gradient in the radial distribution of the scattered light and suggested that curved cavities could provide a better fit to the data. Stapelfeldt et al. (1998b) modeled T Tau's scattered light pattern assuming single scattering in a TSC envelope and investigated what viewing angle and cavity curvature is required to match their *HST* images. They estimated the inclination of the system to be in the range $i=25°$ to 45° with curved cavities ($z=ar^b$, $a=5\times10^{-3}$, and $b=1.95$). Figure 2*b* shows the axisymmetric, single-source model of Stapelfeldt et al. (1998b). The scattered light distribution in the model is necessarily symmetric and does not reproduce the strong asymmetry observed in the WFPC2 image.

4.1.2. *New Three-dimensional Model*

A binary system with shadowing caused by misaligned circumstellar disks may yield a scattered light pattern such as that observed in T Tau. Indeed, Stapelfeldt et al. (1998b) suggested that the unseen secondary may play an important role in forming the scattered light pattern. We have therefore constructed a scattered light model for T Tau incorporating illumination from a binary star system and allowed the alignment of the circumstellar disks to depart from coplanarity.

Our modeling of T Tau begins with the axisymmetric TSC envelope model of Whitney & Hartmann (1993) with the curved cavities derived by Stapelfeldt et al. (1998b), and we adopt $i=40°$, which results in a visual extinction through the envelope to the primary of $A_V\approx2$, close to the observed value. However, in our model the axisymmetry is broken by the illuminating sources. The illumination is by a binary star-plus-disk system where the primary source is aligned with the rotational axis of the envelope and the secondary (larger bolometric luminosity) has its disk aligned so that its polar axis points toward one side of the cavity wall. The direction of the secondary's axis is chosen to agree with the large outflow discovered by Reipurth, Bally, & Devine (1997), which is believed to originate from the secondary.

We assume that the secondary emits 1.5 times as many photons as the primary, based on their estimated bolometric luminosity ratio. The secondary is located 90 AU from the primary in the envelope's equatorial plane, with its disk rotational axis at $\phi=-120°$, $\theta=70°$ (where θ and ϕ are the usual polar coordinates). For our adopted viewing angle the secondary disk is edge-on to our line of sight, and consequently its direct light is highly extincted at optical wavelengths, consistent with its very red spectral energy distribution. Furthermore, the disk orientation blocks the light from the secondary from reaching one side of the cavity. In this model we assume that the primary and secondary are within the same cavity, created by a combination of outflows from both sources.

In Figures 2*c* and 2*d* we show new three-dimensional scattered light models that better reproduce the observed scattered light image of T Tau. We rotated these model images by 20° to allow for comparison with the WFPC2 data. The model in Figure 2*c* shows the scattered light pattern when the illumination is by misaligned circumstellar disks, where the angular dependence of the illumination for each star-plus-disk system is that of the WH92 model in Figure 1. The nonaxisymmetric illumination yields an asymmetric nebula with one side brighter than the other, similar to what is observed. Direct light from the secondary is blocked because of our adopted edge-on orientation of its circumstellar disk, consistent with the lack of observed optical light from the secondary.

In Figure 2*d* we allowed the secondary's illumination pattern to depart from that of the WH92 star-plus-disk of

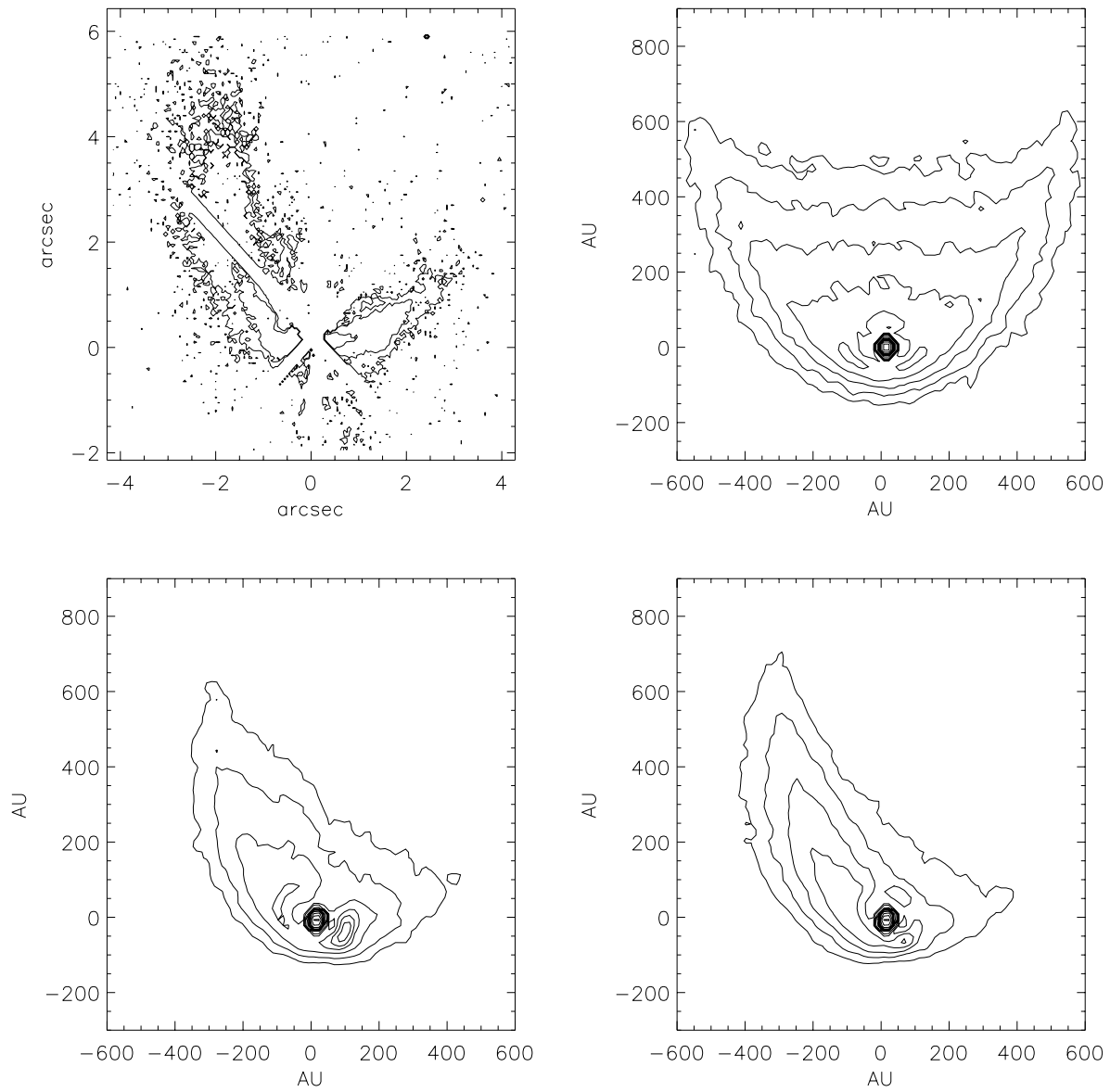

FIG. 2.—(*a*, *top left*) WFPC2 *V*-band (F555W) image of T Tau. (*b*, *top right*) Axisymmetric, single-source, scattered light model of Stapelfeldt et al. (1998b). (*c*, *bottom left*) Scattered light model adopting axisymmetric envelope plus cavities, but with illumination from WH92 star-plus-disks (Fig. 1). The primary is relatively unobscured and its disk rotation axis is aligned with the rotation axis of the TSC envelope. The secondary is oriented so that it is edge-on to our line of sight, and its rotation axis points toward the upper left corner in this figure, breaking the axisymmetry of the illumination and yielding the asymmetric scattered light image. (*d*, *bottom right*) Same as (*c*), but the secondary has a more extreme angular distribution (see Fig. 1), yielding a larger asymmetry in the scattered light image. The images in Figs. 2*c* and 2*d* have been rotated clockwise by 20°; all models are viewed at $i = 40°$. In all panels the contours are at half-magnitude intervals.

Figure 1, in order to investigate whether we could increase the asymmetry in our scattered light models. In this model, the illumination pattern from the secondary is more concentrated toward the polar regions (see Fig. 1). Such an illumination may arise if the secondary's circumstellar material is arranged in a highly flared disk (see, e.g., Chiang & Goldreich 1999) or a small envelope (Roddier et al. 2000). With the more extreme illumination pattern, the asymmetry of the model scattered light nebula is enhanced.

4.1.3. *Efficacy and Limitations of Three-dimensional Model*

Our model for T Tau resembles the WFPC2 image in that it reproduces the asymmetry in the scattered light nebula. Support for our model may be found in observations that show a very complex pattern of outflows in CO (Schuster, Harris, & Russell 1997; Levreault 1988) and molecular hydrogen (Herbst et al. 1996; van Langevelde et al. 1994). As with IRAS 04016+2610 (see below), the plethora of emission knots and filaments is suggestive of a precessing jet and/or multiple outflow sources. The most compelling support for the orientation of the secondary in our models is that its disk axis is aligned with the direction of the outflow discovered by Reipurth et al. (1997) and attributed to the secondary.

In our model the circumstellar disk axes are offset from one another, the primary is viewed at a low inclination, and the secondary is oriented close to edge-on to our line of sight. This is not an unreasonable assumption, given the fact that the secondary in the T Tau system is undetected at optical wavelengths. Also, a system with such a geometry has been observed in the binary HK Tau, where the primary is seen directly and the secondary's scattered light

nebula indicates a highly inclined circumstellar disk (Stapelfeldt et al. 1998a; Koresko 1998).

The inclusion of a secondary source not only breaks the asymmetry in the scattered light image but also increases the contrast between the bright cavity walls and the region interior to this. In their axisymmetric modeling, Stapelfeldt et al. (1998b) produced a contrast no greater than about 2 between the nebular arc and the inner region, whereas the WFPC2 image shows a contrast in excess of 4. Our models can produce contrasts in excess of 4, as shown in Figure 3. This figure shows horizontal intensity cuts at various offsets across the axisymmetric model (Fig. 2*b*) and our new model (Fig. 2*d*). The larger brightness contrast of our non-axisymmetric model (*solid line*), compared with that of the axisymmetric model (*dashed line*), is clearly evident.

While the overall agreement between our V model and the WFPC2 image is very good, we cannot reproduce the thickness of T Tau's nebular arc. This discrepancy is also present in the model of Stapelfeldt et al. (1998b). In our model we have assumed that T Tau's IR companion is a disk source seen almost edge-on. However, because it is undetected in the optical but bright in the IR, we may be viewing at grazing incidence through the upper layers of a flared disk or envelope. If so, detailed three-dimensional modeling of the spectral energy distribution will help in refining our model. We are currently developing techniques for such three-dimensional radiative equilibrium modeling within our Monte Carlo codes (Bjorkman & Wood 2001).

4.2. *IRAS 04016+2610*

4.2.1. *Previous Two-dimensional Models and Evidence for Source Asymmetry*

IRAS 04016+2610 is a Taurus Class I source with a bolometric luminosity of 3.7 $L_{\odot}$ (Kenyon & Hartmann 1995) and displays a very complex scattered light pattern

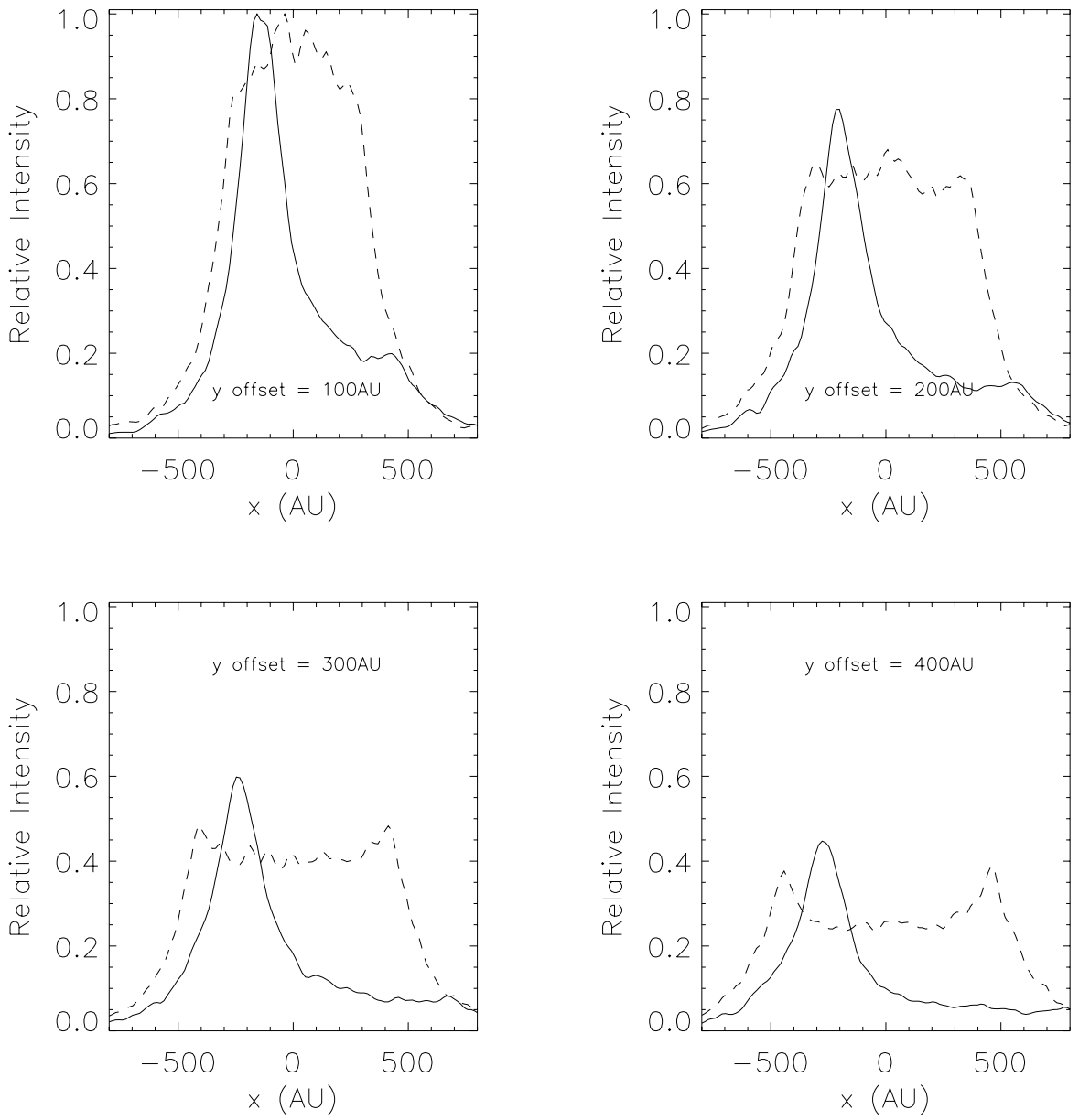

FIG. 3.—Horizontal cuts at various offsets across the scattered light images from Fig. 2*b* (axisymmetric model, *dashed line*) and Fig. 2*d* (asymmetric illumination model, *solid line*). Note the larger intensity contrast of the asymmetric illumination model.

(Whitney et al. 1997; Lucas & Roche 1997; Padgett et al. 1999; Lucas et al. 2000). The Herbig-Haro knots mapped by Gómez, Whitney, & Kenyon (1997) appear scattered throughout the environs, indicative of a precessing jet or multiple outflows. Evidence in favor of multiple outflows is found in the $C^{18}O$ molecular line profiles of Zhou et al. (1994), which show multiple peaks, both red- and blue-shifted. Perhaps the most compelling evidence of multiple outflows is the near-IR imaging polarimetry presented by Lucas & Roche (1997, their Fig. 11) and Whitney et al. (1997, their Fig. 3). Lucas & Roche presented contours of polarized flux (essentially mapping the scattered light), which they interpreted as arising from scattering in an envelope with *two* sets of dust-filled bipolar outflow cavities with projected axes that are almost perpendicular to one another. Our WIYN *I*-band image (shown in Fig. 4*a*) displays bright, elongated limbs that are aligned with the directions of the suspected outflow cavities mapped by Lucas & Roche (1997).

In previous axisymmetric modeling of IRAS 04016+2610, Kenyon et al. (1993a, 1993b) obtained a good match to the spectral energy distribution and low-resolution near-IR imagery adopting a TSC envelope with bipolar, streamline cavities viewed at $i = 60°$. Whitney et al. (1997) adopted a similar model ($\dot{M} = 5 \times 10^{-6}\ M_\odot\ \mathrm{yr}^{-1}$, $r_c = 50$ AU) for their near-IR imaging polarimetry and found that, while it yielded colors close to those observed, to match the observed nebular pattern would require a fully three-dimensional model (as further demonstrated by Lucas & Roche 1997; Lucas et al. 2000). A single, wide, outflow cavity cannot reproduce the distinct V shape in the WIYN image and imaging polarimetry. A single cavity results in a conical scattered light image, but cannot reproduce the large brightness contrast between the arms of the V shape and the interior region; see, e.g., the axisymmetric T Tau model (Fig. 2*b*) and also Whitney & Hartmann (1993) and Stapelfeldt et al. (1998b).

4.2.2. *New Three-dimensional Model*

In our three-dimensional modeling of IRAS 04016+2610 we adopt the TSC envelope geometry and test the multiple-cavity scenario proposed by Lucas & Roche (1997). The TSC envelope has $\dot{M} = 5 \times 10^{-6}\ M_\odot\ \mathrm{yr}^{-1}$ and $r_c = 50$ AU (Whitney et al. 1997). Our scattered light model, shown in Figure 4, has two sets of bipolar, cylindrical, dust-filled cavities carved in the TSC envelope. The primary cavity (aligned along the rotation axis of the TSC envelope) has a radius of 50 AU and the secondary cavity has a radius of 80 AU. The viewing angle is $i = 50°$ relative to the primary cavity. Both cavities have a *J*-band optical depth of 2 measured from the center of the envelope along the cavity axis. To match the bright, elongated limbs in the WIYN image,

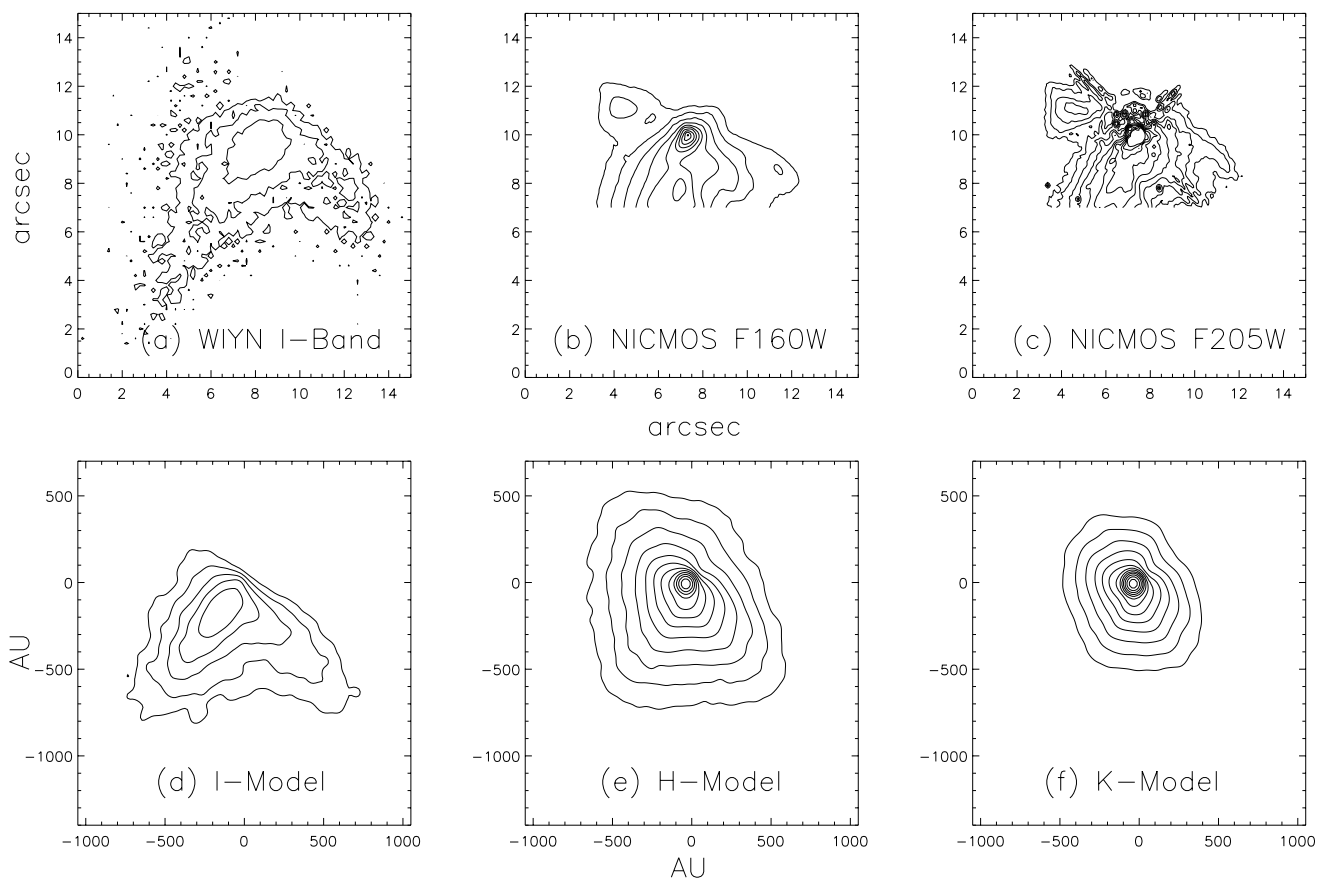

FIG. 4.—Scattered light images and models for IRAS 04016+2610. (*a*) WIYN *I*-band image. (*b*) NICMOS F160W image. (*c*) NICMOS F205W image. Panels (*d*), (*e*), and (*f*) show our scattered light models at *I*, *H*, and *K* bands for a TSC envelope with *two* sets of cylindrical bipolar outflow cavities (see text and Fig. 5). All panels have contours at half-magnitude intervals, and the image and model panels are the same physical size, adopting a distance to IRAS 04016+2610 of 140 pc, so 1″ = 140 AU. The scattered light images have been rotated clockwise by 220° so that the scattered light pattern formed by the primary cavity (aligned with the TSC rotation axis) is aligned with the primary outflow cavity identified labeled by Lucas et al. (2000, their Fig. 2). The models are viewed at an inclination of $i = 60°$ from the primary outflow cavity.

we rotated the axis of the second bipolar cavity to lie along $\phi = -85°$, $\theta = 80°$ (see Fig. 5). In this model the two bipolar cavities are almost perpendicular, as noted by Lucas & Roche (1997). The scattered light images have been rotated clockwise by 220° so that the scattered light pattern formed by the primary cavity (aligned with the TSC rotation axis) is aligned with the primary outflow cavity identified by Lucas & Roche (1997; see the labeling in Fig. 2 of Lucas et al. 2000).

Lucas & Roche (1997) interpreted their data as possible evidence for a binary carving two outflow cavities. Following their lead, we have adopted an unresolved binary for the illuminating sources. The NICMOS images of Padgett et al. (1999) and centimeter observations of Lucas et al. (2000) did not resolve a binary companion. We also constructed a model with the two outflow cavities described above but with illumination from a single source. Because the disk sources depart from isotropy only along equatorial directions (Fig. 1), we found that the scattered light pattern from a single source is not distinguished from that of the unresolved binary model of Fig. 4. Therefore, unlike our T Tau model, we infer that for IRAS 04016+2610 it is the envelope structure that is most important in producing the image morphology and not asymmetric illumination.

4.2.3. *Efficacy and Limitations of Three-dimensional Model*

Our model reproduces the overall size and morphology of the WIYN and NICMOS images very well. In the *I*-band model, the envelope is optically thick, and it is the cavities that dominate the image morphology. However, at optically thinner, longer wavelengths the envelope structure is important in shaping the resulting image. Our model has a single TSC envelope with the primary cavity along the rotation axis and the second cavity almost perpendicular to this. If the source is indeed a binary, then the envelope geometry is likely different from that of TSC. Indeed, recent modeling of imaging spectroscopy by Hogerheijde (2001) adopted a 2000 AU radius axisymmetric rotating disklike structure. Such a "disk" should not be confused with the smaller circumstellar disks that we adopt and that are seen in other classical T Tauri stars (see, e.g., Burrows et al. 1996; Padgett et al. 1999). The TSC rotational collapse geometry produces a large equatorial density enhancement, which may correspond to Hogerheijde's parameterized equatorial structure. If so, the equatorial enhancement of TSC and Hogerheijde's "disk" represent a different evolutionary stage from disks around classical T Tauri stars (Shu et al. 1987). A more detailed model of IRAS 04016+2610 than we have undertaken should simultaneously address the envelope geometry and velocity structure. Nevertheless, our models, which incorporate the TSC parameters determined by Kenyon et al. (1993b) and Whitney et al. (1997), provide support for Lucas & Roche's (1997) dual bipolar cavity interpretation of their imaging polarimetry.

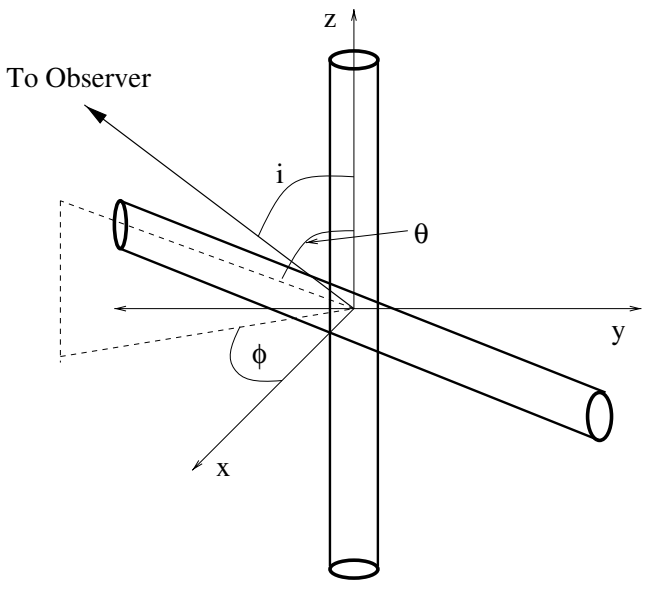

FIG. 5.—Schematic of the outflow cavity geometry and orientation used in our model of IRAS 04016+2610 (Fig. 4).

Our model colors are $J'-H' = 1.34$ and $H'-K' = 0.79$, giving actual colors of $J-H = 2.11$ and $H-K = 1.22$ when combined with the adopted intrinsic colors (§ 3.5). The observed colors for IRAS 04016+2610 are $J-H = 1.95$ and $H-K = 2.02$ (Kenyon & Hartman 1995; Whitney et al. 1997). The failure of both our models and those of Whitney et al. (1997) to reproduce these colors (both models predict $J-H > H-K$) may indicate that the intrinsic source colors are different from those we have adopted.

While we have been successful in reproducing the image morphology, our models suffer from the same problem as those of Whitney et al. (1997) in that they predict lower polarizations than observed. Whitney et al. attribute this to the low intrinsic polarization of the KMH grains. In our case, the resolved polarization is lower than observed because of the dust grains, but we also find much lower levels for the total unresolved polarization in our models. We typically predict an integrated polarization of around 3% in the near-IR, whereas the observed polarization ranges from $P_J = 21\%$ to $P_K = 8\%$ (Whitney et al. 1997). Another problem is that neither our models nor those of Whitney et al. (1997) can reproduce the observed pattern of polarization vectors close to the source(s). So, while the dual-cavity scenario proposed by Lucas & Roche (1997) gives a good match to the overall image morphology, its failure to reproduce the observed polarization level and pattern in IRAS 04016+2610 indicates that the details of the model need to be refined. In particular, polarization due to scattering off aligned grains can yield larger polarization values, and we are investigating grain alignment in protostars to reconcile models with the large observed polarizations (Whitney & Wolff 2001, in preparation).

5. SUMMARY OF RESULTS

We have constructed three-dimensional models for the scattered light nebulae associated with IRAS 04016+2610 and T Tau. Our models assumed an axisymmetric infalling circumstellar envelope, but the axisymmetry was broken by multiple outflow cavities and nonaxisymmetric illumination from binary stars.

The asymmetry seen in the nebula surrounding T Tau was modeled by introducing a secondary star-plus-disk system with its rotation axis misaligned from the axis of the TSC envelope. The orientation of the secondary was chosen so that its disk was almost edge-on to our line of sight and perpendicular to the Herbig-Haro outflow attributed to the secondary (Reipurth et al. 1997). This orientation results in the secondary being undetected in our scattered light models because its disk extincts the direct optical light.

We reproduced the scattered light pattern associated with IRAS 04016+2610 with a model with two sets of bipolar outflow cavities in the TSC envelope. This model affirms the notion of Lucas & Roche (1997), who interpreted their near-IR imaging polarimetry as arising from scattering in an envelope with orthogonal bipolar cavities. Further evidence for multiple cavities in the envelope is found in the complex pattern of outflow emission knots surrounding this source (Gómez et al. 1997). Our model fails, however, to reproduce the level and pattern of the near-IR polarization, and we suspect that a more accurate treatment of polarization from scattering off aligned grains may provide a better match to the observations (Whitney & Wolff 2001, in preparation).

In the models presented in this paper, we adopted the axisymmetric TSC solution for the circumstellar envelopes. This may not be appropriate, because T Tau is a known binary and IRAS 04016+2610 shows strong evidence for binarity. Also, other studies indicate that protostellar environments have material arranged with a shallower radial gradient than TSC (see, e.g., Barsony & Chandler 1993). The extension of our Monte Carlo scattering codes to three dimensions now enables us to incorporate more complex circumstellar envelope structures, such as those predicted from binary star formation models. However, this is among the first modeling investigations to explore the effects of three-dimensional cavity structures and illuminations, and it has proved successful in reproducing the scattered light morphologies and in testing several scenarios proposed by others to explain the observations. While we have been fairly successful in reproducing the scattered light morphologies, spectral energy distribution modeling incorporating the three-dimensional structures will provide a crucial test of our models. This requires current axisymmetric radiation transfer radiative equilibrium codes to be extended to three dimensions, and we are developing such techniques (Bjorkman & Wood 2001).

We acknowledge financial support from NASA's Long-Term Space Astrophysics Research Program, NAG 5-6039 (K. W.) and NAG 5-8412 (B. W.); the National Science Foundation, AST 99-09966 (B. W. and K. W.); the *HST* Archival Research Program AR-08367.01-97A (B. W., K. W., K. S.); and NASA's Astrophysical Data Program, NAG 5-3904 (M. J. W.). K. S. B. is a Cottrell Scholar of the Research Corporation, and gratefully acknowledges their support. D. S. S. was funded by the NSF Research Experience for Undergraduates program at the Harvard-Smithsonian Center for Astrophysics and thanks Christine Jones, Jonathan McDowell, and Tania Ruiz for the generous donation of time and self to make the SAO Intern Program as rewarding as it has been. We thank Karl Stapelfeldt for providing the WFPC2 image of T Tau and Ted von Hippel for assistance with the WIYN queue observations.

REFERENCES

Adams, F. C., Lada, C. J., & Shu, F. H. 1987, ApJ, 312, 788
Adams, F. C., & Shu, F. H. 1986, ApJ, 308, 836
Barsony, M., & Chandler, C. J. 1993, ApJ, 406, L71
Bastien, P., & Ménard, F. 1990, ApJ, 364, 232
Beckwith, S. V. W., & Sargent, A. I. 1991, ApJ, 381, 250
Beckwith, S. V. W., Sargent, A. I., Chini, R. S., & Güsten, R. 1990, AJ, 99, 924
Beichman, C. A., Myers, P. C., Emerson, J. P., Harris, S., Mathieu, R., Benson, P. J., & Jennings, R. E. 1986, ApJ, 307, 337
Bergeron, L. E., & Skinner, C. J. 1997, AAS, 191, 10.04
Bjorkman, J. E., & Wood, K. 2001, ApJ, 554, 615
Burrows, C. J., et al. 1996, ApJ, 473, 437
Chiang, E. I., & Goldreich, P. 1999, ApJ, 519, 279
Code, A. D., & Whitney, B. A. 1995, ApJ, 441, 400
Cohen, M., Emerson, J. P., & Beichman, C. A. 1989, ApJ, 339, 455
Dyck, H. M., Simon, T., & Zuckerman, B. 1982, ApJ, 255, L103
Fischer, O., Henning, T., & Yorke, H. W. 1994, A&A, 284, 187
Ghez, A. M., Neugebauer, G., Gorham, P. W., Haniff, C. A., Kulkarni, S. R., Matthews, K., Koresko, C., & Beckwith, S. 1991, AJ, 102, 2066
Gómez, M., Whitney, B. A., & Kenyon, S. J. 1997, AJ, 114, 1138
Hartmann, L., Calvet, N., Allen, L., Chen, H., & Jayawardhana, R. 1999, AJ, 118, 1784
Henyey, L. G., & Greenstein, J. L. 1941, ApJ, 93, 70
Herbst, T. M., Beckwith, S. V. W., Glindemann, A., Tacconi-Garman, L. E., Kroker, H., & Krabbe, A. 1996, AJ, 111, 2403
Hogerheijde, M. R. 2001, ApJ, 553, 618
Kenyon, S. J., Calvet, N., & Hartmann, L. 1993a, ApJ, 414, 676
Kenyon, S. J., Gómez, M., Marzke, R. O., & Hartmann, L. 1994, AJ, 108, 251
Kenyon, S. J., & Hartmann, L. 1995, ApJS, 101, 117
Kenyon, S. J., Hartmann, L., Strom, K. M., & Strom, S. E. 1990, AJ, 99, 869
Kenyon, S. J., Whitney, B. A., Gómez, M., & Hartmann, L. 1993b, ApJ, 414, 773
Kim, S.-H., Martin, P. G., & Hendry, P. D. 1994, ApJ, 422, 164 (KMH)
Koresko, C. D. 1998, ApJ, 507, L145
Krist, J. E. 1995, in Calibrating *Hubble Space Telescope*: Post Servicing Mission, ed. A. Koratkar & C. Leitherer (Baltimore: STScI), 311
Krist, J. E., et al. 1999, ApJ, 515, L35
———. 1998, ApJ, 501, 841
Lada, C. J. 1987, in IAU Symp. 115, Star-Forming Regions, ed. M. Peimbert & J. Jugaku (Dordrecht: Kluwer), 1
Lada, C. J., & Wilking, B. A. 1984, ApJ, 287, 610
Levreault, R. M. 1988, ApJS, 67, 283
Lucas, P. W., Blundell, K. M., & Roche, P. F. 2000, MNRAS, 318, 526
Lucas, P. W., & Roche, P. F. 1998, MNRAS, 299, 699
Lucas, P. W., & Roche, P. F. 1997, MNRAS, 286, 895
Myers, P. C., Fuller, G. A., Mathieu, R. D., Beichman, C. A., Benson, P. J., Schild, R. E., & Emerson, J. P. 1987, ApJ, 319, 340
Padgett, D. L., Brandner, W., Stapelfeldt, K. R., Strom, S. E., Terebey, S., & Koerner, D. 1999, AJ, 117, 1490
Reipurth, B., Bally, J., & Devine, D. 1997, AJ, 114, 2708
Reipurth, B., Yu, K. C., Heathcote, S., Bally, J., & Rodríguez, L. F. 2000, AJ, 120, 1449
Roddier, C., Roddier, F., Graves, J. E., Northcott, M. J., Close, L., Surace, J., & Véran, J. P. 1999, in ESO Conference and Workshop Proceedings 56, Astronomy with Adaptive Optics: Present Results and Future Programs, ed. D. Bonaccini (Garching: ESO), 389
Roddier, F., Roddier, C., Brandner, W., Charissoux, D., Véran, J. P., & Courbin, F. 2000, in Birth and Evolution of Binary Stars, Poster Proceedings of IAU Symp. 200 on The Formation of Binary Stars, Birth and Evolution of Binary Stars, ed. B. Reipurth & H. Zinnecker (Potsdam: Astrophys. Inst.), 60
Schuster, K.-F., Harris, A. I., & Russell, A. P. G. 1997, A&A, 321, 568
Shu, F. H., Adams, F. C., & Lizano, S. 1987, ARA&A, 25, 23
Stapelfeldt, K. R., Krist, J. E., Ménard, F., Bouvier, J., Padgett, D. L., & Burrows, C. J. 1998a, ApJ, 502, L65
Stapelfeldt, K. R., et al. 1999, ApJ, 516, L95
———. 1998b, ApJ, 508, 736
———. 1995, ApJ, 449, 888
Strom, S. E. 1994, Rev. Mexicana Astron. Astrofis., 29, 23
Tamura, M., Gatley, I., Joyce, R. R., Ueno, M., Suto, H., & Sekiguchi, M. 1991, ApJ, 378, 611
Terebey, S., Shu, F. H., & Cassen, P. 1984, ApJ, 286, 529 (TSC)
Terebey, S., van Buren, D., Padgett, D. L., Hancock, T., & Brundage, M. 1998, ApJ, 507, L71
van Langevelde, H. J., van Dishoeck, E. F., van der Werf, P. P., & Blake, G. A. 1994, A&A, 287, L25
Weintraub, D. A., Kastner, J. H., Zuckerman, B., & Gatley, I. 1992, ApJ, 391, 784
Whitney, B. A., & Hartmann, L. 1993, ApJ, 402, 605
———. 1992, ApJ, 395, 529
Whitney, B. A., Kenyon, S. J., & Gómez, M. 1997, ApJ, 485, 703
Wilking, B. A., Lada, C. J., & Young, E. T. 1989, ApJ, 340, 823
Witt, A. N. 1977, ApJS, 35, 1
Wood, K., & Reynolds, R. 1999, ApJ, 525, 799
Wood, K., Crosas, M., & Ghez, A. M. 1999, ApJ, 516, 335
Yusef-Zadeh, F., Morris, M., & White, R. L. 1984, ApJ, 278, 186
Zhou, S., Evans, N. J., II, Wang, Y., Peng, R., & Lo, K. Y. 1994, ApJ, 433, 131